# Finite Element Approach to Microwave Sintering of Oxide Materials

Yuhua Duan[1,2*], Dan C. Sorescu[1] and J. Karl Johnson[1,3]
[1] National Energy Technology Laboratory, U.S. Department of Energy, Pittsburgh, PA 15236
[2]Parsons Project Services Inc., South Park, PA 15129
[3]Department of Chemical Engineering, University of Pittsburgh, Pittsburgh, PA 15261

*Corresponding author: duany@netl.doe.gov

**Abstract:** Microwave sintering has been applied to a wide variety of materials during the past three decades as an alternative to conventional thermal sintering. Recent experimental results showed that for semimetal or magnetic materials the magnetic field (**H**) can have a significantly larger contribution than the electric field (**E**) during sintering. We have employed the COMSOL Multiphysics™ package to simulate the sintering process by adding the magnetic field contribution into the heating source. We performed simulations with both **E** and **H** fields or with isolated **E** or **H** fields. For the systems of $Fe_3O_4$, $Al_2O_3$ and ZnO oxides, our simulated results are in good qualitative agreement with the experimental sintering findings. We also explored the sintering of nano-size ZnO/γ-$Fe_2O_3$ and macro-size ZnO/γ-$Al_2O_3$ composite particles.
**Keywords:** Microwave Sintering, Finite Element Method, Conventional heating, COMSOL

## 1. Introduction

Conventional thermal sintering technology has been used for centuries to make different kinds of objects from powdered materials. The use of microwaves to process electromagnetic absorbing materials has been studied since the 1970s and has now been applied to a wide variety of materials [1], including wood, foodstuffs, rubber, ceramics, semiconductors and metals[2]. Microwave sintering can result in materials with different micro-structures and enhanced properties compared with conventional sintering[3]. Moreover, microwave sintering requires much less energy than conventional methods.

Although microwave technology has been used in sintering processes for many years, its mechanism is still not well understood, especially regarding the effects of the magnetic field of the electromagnetic wave. In the literature, dielectric properties are considered as main heating source during microwave sintering and the contribution from magnetic energy losses are ignored. However, recent experimental results showed that the magnetic field is also very important during microwave sintering, especially for sintering of ferromagnetic/magnetic materials and semi-metal/metal composite materials [3,4]. For sintering these materials, by separating the electric field (**E**) and magnetic field (**H**), the experiments revealed that the magnetic field **H** can also play an important role in the heating process [3,4]. Unfortunately, as far as we know there are no theoretical studies or simulations that consider both contributions from **E** and **H** fields in microwave heating. Instead, most of the previous theoretical work just treated sintering by considering only the dielectric contributions and assumed that the contributions from magnetic energy loss are very small and consequently can be ignored [5-7].

In this paper, we include all the heating sources from electromagnetic wave and perform a finite element simulation with the COMSOL Multiphysics™[8] to explore the mechanism of microwave sintering. In the next section, we briefly describe our simulation procedure. Then we present calculations for several types of oxides and their composites and compare our results with the available experimental findings. In the last section, we summarize our results and conclusions.

## 2. Simulation Methods and Procedures

In this work we consider only two dimensional (2D) microwave sintering geometries in order to simplify the calculations. Figure 1 shows our simulation model which is a simplified version of the experimental setup described in ref. [1]. In this 2D model [8], the cylindrical sample is placed in an insulating powder which is surrounded by porous materials. For the electromagnetic propagation and heat transfer modules, the boundary conditions are different. In the heating transfer module, the heat transfer from sample into insulation powder, and then to the air, therefore, the boundary condition between the powder and air was taken to be the heat flux. In the electromagnetic module, we apply the electromagnetic wave from top and bottom in our

2D model while the boundary conditions were set to port options in COMSOL package. The boundary between the powder and the air is taken as a perfect conductor as shown in Fig. 1. Since the enclosure atmosphere can influence the thermal and electrical properties of the ceramic sintering, here for simplicity we consider an air atmosphere in all our simulations.

In this 2D axisymmetric model shown in Fig.1, we combine the propagation equation of the electromagnetic waves ($TM_{01}$ or TE mode, correlated by Faraday's law) with the heat transfer equation in order to get the sintering temperature distributions and other system properties. The propagation of electromagnetic waves is governed by the following equation (1) or (2), corresponding to TM or TE mode respectively.

$$\nabla \times [\varepsilon_r^{-1}(\mathrm{T}) \cdot \nabla \times \mathbf{H}] - \omega^2 \mu_r(\mathrm{T})\mathbf{H} = 0 \quad (1)$$

$$\nabla \times [\mu_r^{-1}(\mathrm{T}) \cdot \nabla \times \mathbf{E}] - \omega^2 \varepsilon_r(\mathrm{T})\mathbf{E} = 0 \quad (2)$$

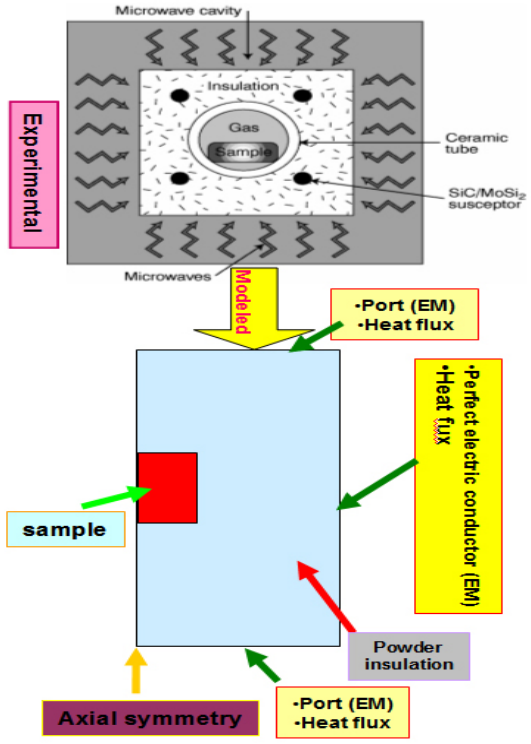


**Fig.1**. The simulation model for microwave sintering based on the experimental apparatus [1,2,8].

where ω is the electromagnetic wave frequency. The permittivity $\varepsilon_r$ and permeability $\mu_r$ are complex parameters of the form: $\varepsilon_r = \varepsilon' - j\varepsilon''$ and $\mu_r = \mu' - j\mu''$.

By applying standard boundary conditions and using finite element methods, one can solve either equations (1) or (2) to obtain the distribution of the **E** and **H** fields. The power flux associated with propagating electromagnetic waves is represented by the Poynting vector **S** which is defined as [5,9]

$$\mathbf{S} = \frac{1}{2}\mathbf{E} \times \mathbf{H}^* \quad (3)$$

The Poynting theorem allows the evaluation of the electromagnetic power dissipated in the medium. This dissipated power is the total heating source in the sintering process. The total heating source ($\dot{q}$) includes the Joule resistive loss and the electromagnetic power dissipated per unit volume, as given by the following formula:

$$\dot{q} = \sigma \mathbf{E} \cdot \mathbf{E}^* - \mathrm{Re}(\nabla \cdot \mathbf{S})$$

$$= \sigma \mathbf{E} \cdot \mathbf{E}^* + \frac{1}{2}\omega(\varepsilon_r'' \mathbf{E} \cdot \mathbf{E}^* + \mu_r'' \mathbf{H} \cdot \mathbf{H}^*) \quad (4)$$

In eq. (4), the first term is the resistive loss from Joule's law, and the 2nd and 3rd terms are the electric and magnetic energy losses from the electromagnetic field. $\mathbf{H}^*$ and $\mathbf{E}^*$ denote the conjugate quantities of **H** and **E** fields. In eqs. (1), (2) and (4), the permittivity ($\varepsilon_r$) and permeability ($\mu_r$) are complex parameters and are temperature and frequency dependent. From eq.(4) one can see that electromagnetic energy losses are dominated by the **E** and **H** fields and depend also on the imaginary parts of permittivity and permeability parameters, ε" and μ". All calculations in this study have been performed using a microwave field of 2.5GHz. In Table 1 are listed the complex $\varepsilon_r$ and $\mu_r$ parameters for several oxides which were used in our simulations.

**Table 1. Complex permittivity & permeability For some oxides at frequency 2.5GHz**

| Materials | ε' | ε'' | μ' | μ'' | Refs. |
|---|---|---|---|---|---|
| $Fe_3O_4$ | 25.0 | 3.1 | 7.5 | 2.0 | [10] |
| $Al_2O_3$ | 3.006 | 0.17 | 1.0 | 0.02 | [11] |
| ZnO | 4.0 | Vary with T | 1.0 | 0.01 | [12] |
| ZnO/γ-$Fe_2O_3$ | 6.6 | 0.5 | 1.2 | 1.3 | [13] |
| Powder, Air | 1.0 | 0.0 | 1.0 | 0.0 | |

From Table 1 one can see that for the powder we set the values of ε' and μ' to 1.0 and the values of ε" and μ" to zero. This simplification means that

they only act as heat transfer media. From our investigations, we found that the parameters $\varepsilon_r$ and $\mu_r$ (especially their imaginary parts) are very sensitive to the heating profile.

The heat transfer can be described by equation

$$\rho C_p \frac{\partial T}{\partial t} - \nabla \cdot \kappa \nabla T = \dot{q} \qquad (5)$$

where $\rho$ is the density, $C_p$ is the heat capacity, $\kappa$ is the heat transfer coefficient, $T$ is temperature, $t$ is the time. These parameters can be readily found in handbooks [14,15].

By solving equation (5) with certain boundary conditions shown in Fig.1, we can get the sintering temperature $T$ distributions in the sample as function of the simulation time $t$.

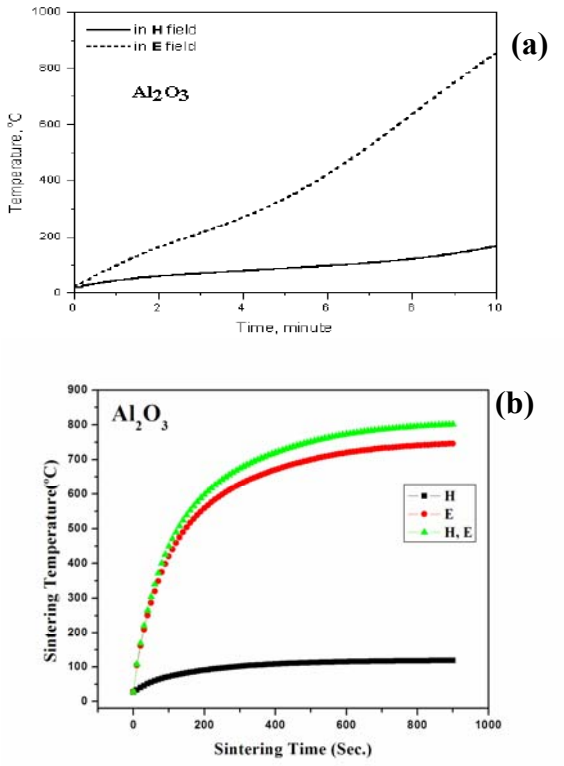


**Fig.2**. The sintering temperature at the center of $Al_2O_3$.
(**a**) experimental results from refs.[3,4].
(**b**) our simulation results with isolated **E** and **H** And with both **E** and **H** fields.

## 3. Results and Discussions

For a given system, we have added the **H**-field contributions (shown in eq.(4)) to the existing **E** contributions in the electromagnetic wave module of COMSOL software [8]. By solving the above equations (1-5) we obtained the sintering temperature distributions and other properties (such as the electric and magnetic energy and flux densities, and the **E** and **H** distributions, etc.). In order to model the experimental procedure in which the **H** and **E** fields are separated [4,16,17], we simply set the values of ε" or μ" to zero and ε' or μ' to 1.0 respectively.

### 3.1 Sintering of $Al_2O_3$

Figure 2 shows our simulation results and the corresponding experimental data [4] for the case of $Al_2O_3$ oxide. It can be seen that in both cases the magnetic field contribution is much smaller than the contribution from the electric field. In this case, electric field plays an important role during sintering. Although the contribution from magnetic field is small, it can not be neglected for accurate description of $Al_2O_3$ sintering.

In agreement with experimental results (Fig. 2(a)), we obtained that the main heating contributions is due to the **E** field (Fig. 2(b)). However, our simulation predicted a much shorter time period to reach the saturation temperature than that determined experimentally. We note, however, that our predicts are in agreement with those obtained in ref. [4] for a series of 14 oxides where saturation has been reached within 10 minutes of irradiation. At this moment we don't have a simple explanation for the difference between $Al_2O_3$ and other oxides investigated in ref.[4].

### 3.2 Sintering of $Fe_3O_4$

The simulated results and the experimental measurements for $Fe_3O_4$ are showed in figure 3. In contrast to the sintering behavior of $Al_2O_3$, both **E** and **H** fields are important for the sintering of $Fe_3O_4$. We note that the contribution from **H**-field is larger than the contribution from **E**-field. This means that the **H** field is dominant during sintering of $Fe_3O_4$. Comparing our simulation results with experimental measurements, it can be seen from figure 3 that they agree with each other very well. $Fe_3O_4$ is a magnetic oxide material and its imaginary part of $\mu_r$ is much bigger than that for $Al_2O_3$. Therefore, it should have a larger magnetic energy loss than $Al_2O_3$ does.

It should be pointed out that the experimental sintering for $Fe_2O_3$ and FeO showed that the electric field **E** plays an important role during sintering of these two oxides [4]. It should be very interesting to find out why the sintering behavior of $Fe_2O_3$ and FeO are different from $Fe_3O_4$, because

the later can be treated as the combination of $Fe_2O_3$ and FeO. Unfortunately, we were unable to find both $\varepsilon_r$ and $\mu_r$ values for $Fe_2O_3$ and FeO systems and therefore, we were unable to perform similar simulation on these oxides.

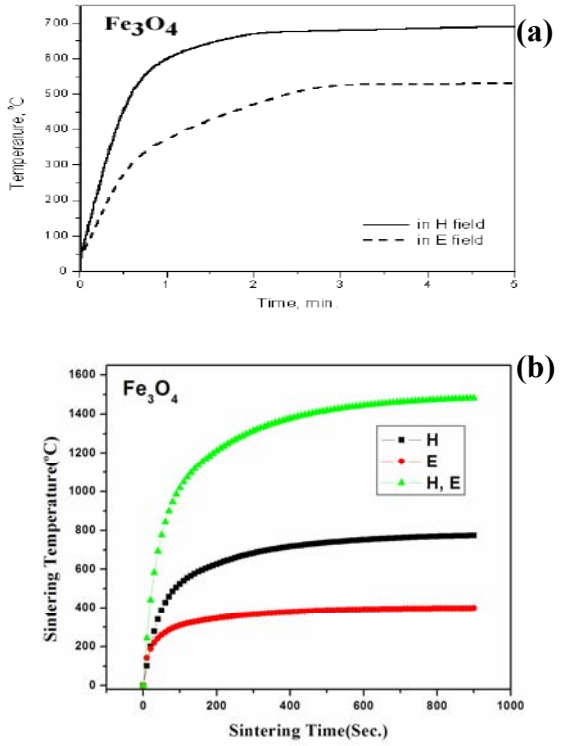


**Fig.3**. The sintering temperature at the center of $Fe_3O_4$.
(**a**) experimental measurements from refs.[3,4]
(**b**) our simulation results with isolated **E** and **H** and with both **E** and **H** fields.

### 3.3 Sintering of ZnO

As we mentioned above, the complex permittivity and permeability are frequency and temperature dependent. Since we fixed our frequency at 2.5GHz, we only need to consider the temperature dependence. For $Al_2O_3$ and $Fe_3O_4$, as described above in Table 1, the measured parameters of $\varepsilon_r$ and $\mu_r$ only show frequency dependence, hence, we have to assume they are constant for all temperatures.

For ZnO, the experimental data for ε" at different temperatures are available [12]. We have used these experimental data in our simulation. For those temperatures where experimental data are not available, we use the interpolation function to create the corresponding value. Figure 4 shows our simulation results and the experimental sintering measurements of ZnO.

From Fig. 4, one can see that both experimental and simulation results show that the **E** field is more important than the **H** field during sintering of ZnO. Comparing with $Al_2O_3$, the **H** field contribution is even smaller. Therefore, it's reasonable to neglect the **H** field contribution during sintering of ZnO and consider only the dielectric contributions.

Comparing Fig.4(a) with Fig.4(b), it can be seen that the simulation results have a depression within the first 5 minutes. The reason for this is that the ε" values vary greatly when $T$<700ºC.

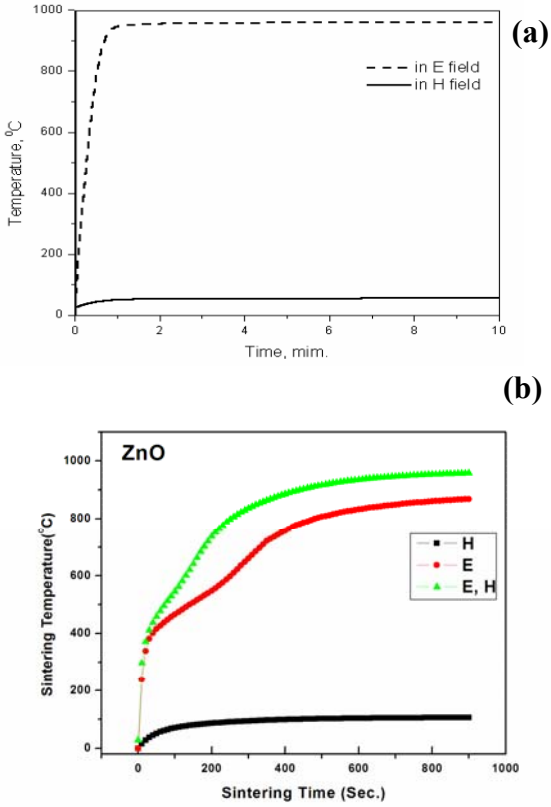


**Fig.4**. The sintering temperature at the center of ZnO.
(**a**) experimental results from refs.[3,4]
(**b**) our simulation results with isolated **E** and **H** and with both **E** and **H** fields.

### 3.4 Sintering of nano-size ZnO/γ-$Fe_2O_3$

The sintering technology has been used widely to make composite materials from different kinds of powder. Talbot *et al*[13] reported measurements of the composition and frequency-dependent of $\varepsilon_r$ and $\mu_r$ for ZnO/γ-$Fe_2O_3$ composites prepared by powder pressing as function of composition and frequency. The electromagnetic properties of these materials exhibit a strong dependence on the powder size of the starting materials. They

investigated nanometer-size and micrometer-size particles and found that their behaviors are different. For the nano-size powder, the material is described by a unique set of $\varepsilon_r$ and $\mu_r$ parameters (Table 1). In this case, we can treat these two kinds of powder as a homogeneous material and apply the same model as described above to do the sintering. Fig. 5 shows our simulation results.

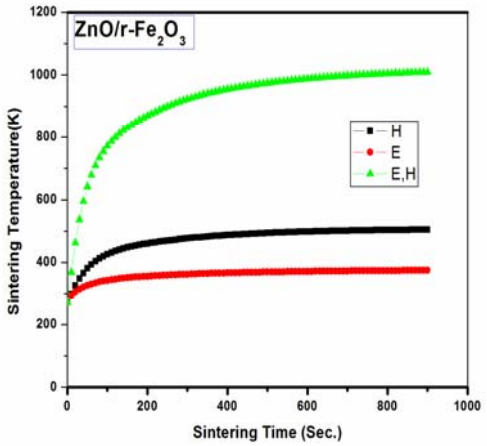


**Fig. 5.** The sintering results for nanosize ZnO with $\gamma$-$Fe_2O_3$, which are treated as a uniform material, under isolated **E** and **H** and under both **E** and **H** fields.

From Fig.5, in sintering this kind of composite material both **H** and **E** fields are important. The contribution from the **H**-field is a little bit larger than that from the **E**-field. It also can be seen that the results with both fields present can not be obtained by linear addition of the results for the single fields. This can be understood based on the nonlinear nature of Maxwell equations. Therefore, the sintering temperature with both fields is normally higher than the sum of **E**-only and **H**-only results.

### 3.5 Sintering of macro-size $ZnO/Al_2O_3$

Based on the available parameters, we build a 2D model for composite $ZnO/Al_2O_3$ particles. Different from the nanosize composie of ZnO/ $\gamma$-$Fe_2O_3$ as described above, composite $ZnO/Al_2O_3$ is heterogeneous and has individual particles with different $\varepsilon_r$ and $\mu_r$ parameters. Figure 6(a) shows our simulating sample scheme. Different from the sample shape shown in Fig.1, the shape of each grain is set as a circle with the diameter of about 1 cm in 2D case, surrounded with powder.

Fig.6(b) and Fig.6(c) give the temperature distributions on each grain along the sintering time t. It can be seen that there are some differences among those grains, especially during the first 100 seconds. The $Al_2O_3$ grains located in the center region have higher temperatures than the other grains.

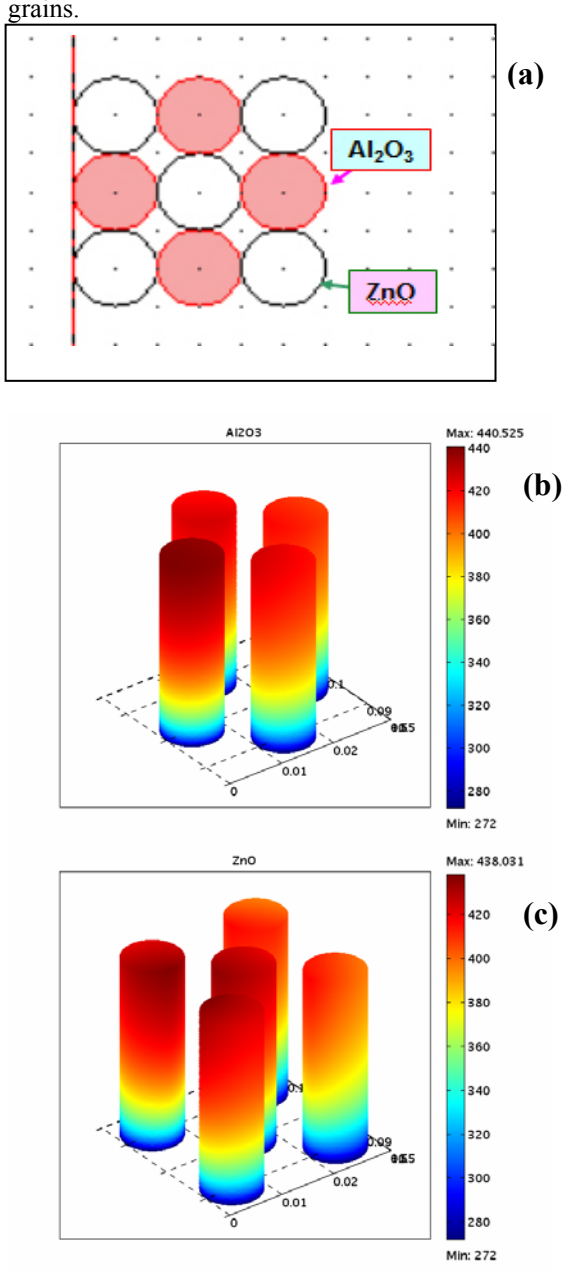


**Fig.6.** The sintering temperature distributions for $Al_2O_3$ and ZnO composites which are treated separately. (a)Sample grains surrounded with powder; (b) $Al_2O_3$; (c) ZnO. The plane is the position axis. Vertical axis is the simulating time from 0 to 900 Sec.

Overall, during the earlier stage of sintering, the $Al_2O_3$ absorbed more heat than ZnO grain and consequently have higher **T** distributions.

Since our input microwave power is too low and the sintering time is also short, we do not reach the melting temperature in this simple modeling. To study the melt interface region, the parameters for the interface must be known as they are expected to be different from those of individual component systems.

## 4. Conclusions and Further Work

From the above discussions, it can be seen that for ZnO, $Al_2O_3$ and their composites the **E** field is more important than the **H** field, whereas for $Fe_3O_4$ and ZnO/γ-$Fe_2O_3$ systems the **H** field plays a more important role during sintering. Our simulation results are in good qualitative agreement with the experimental findings [3,4]. Although both **E** and **H** fields contribute to the heating source, for different materials there may be only one of them which dominates the heating source during microwave sintering. Generally speaking, ferromagnetic or magnetic materials ($Fe_3O_4$, as an example) have larger μ" values and therefore the magnetic energy loss is more important during microwave sintering and can not be neglected; diamagnetic and anti-ferromagnetic materials (eg. $Al_2O_3$ and ZnO) have very small values of μ" and therefore the **E** field plays the dominant role during microwave sintering. It should be pointed out that the sintering temperature is very sensitive to the values of the μ" and ε" parameters, which reflects that in order to achieve good agreement with experimental behavior those parameters must be measured to high precision.

In addition, our simulation results also show that the thermal properties (thermal conductivity, $C_p$, κ, etc.) and the size and shape of sample particles also affect the sintering temperature distributions. Sintering of composite materials and the micro-structure among them are under investigating by combining finite element methods with an atomistic simulation approach.

## References


1. Roy R, Agrawal D, Cheng JP, Gedevanishvili S: **Full sintering of powdered-metal bodies in a microwave field**. *Nature* 1999, **399**:668-670.
2. Sutton W: **Microwave processing of ceramics: an review**. *Mater. Res. Soc. Symp. Proc.* 1992, **269**:3-19.
3. Breval E, Cheng JP, Agrawal DK, Gigl P, Dennis A, Roy R, AJ P: **Comparison between microwave and conventional sintering of WC/Co composites**. *Mater. Sci. Eng. A* 2005, **391**:285-295.
4. Cheng JP, Roy R, Agrawal D: **Radically different effects on materials by separated microwave electric and magnetic fields**. *Materials Research Innovations* 2002, **5**:170-177.
5. Ayappa KG, Davis HT, Crapiste G, Davis EA, Gordon J: **Microwave heating: an evaluation of power formulations**. *Chemical Engineering Science* 1991, **46**:1005-1016.
6. Chatterjee A, Basak T, Ayappa KG: **Analysis of microwave sintering of ceramics**. *AIChE Journal* 1998, **44**:2302-2311.
7. Olevsky EA: **Theory of sintering: from discrete to continuum**. *MATERIALS SCIENCE AND ENGINEERING* 1998, **R23**:41-100.
8. *COMSOL Multiphysics, COMSOL, Inc., Burlington, MA, www.comsol.com*.
9. Campos I, Jimenez JL: **About Poynting's Theorem**. *Eur. J. Phys.* 1992, **13**:117-121.
10. Belhadjtahar NE, Fourrierlamer A, Dechanterac H: **Broad-Band Simultaneous Measurement of Complex Permittivity and Permeability Using a Coaxial Discontinuity**. *Ieee Transactions on Microwave Theory and Techniques* 1990, **38**:1-7.
11. Ma J, Fang M, Li P, Zhu B, Lu X, Lau NT: **Microwave-assisted catalytic combustion of diesel soot**. *Applied Catalysis A: General* 1997, **159**:211-228.
12. Martin LP, Dadon D, Rosen M, Gershon D, Rybakov KI, Birman A, Calame JP, Levush B, Hutcheon R: **Effects of anomalous permittivity on the microwave heating of zinc oxide**. *Journal of Applied Physics* 1998, **83**:432-437.
13. Talbot P, Konn AM, Brosseau C: **Electromagnetic characterization of fine-scale particulate composite materials**. *Journal of Magnetism and Magnetic Materials* 2002, **249**:481-485.
14. **CRC Handbook of Chemistry and Physics**. Edited by Lide DR: CRC Press; 2002.
15. In *Chemical Properties Handbook*. Edited by: McGRAW-Hill; 1998.
16. Cheng JP, Agrawal D, Zhang YJ, Roy R: **Microwave sintering of transparent alumina**. *Materials Letters* 2002, **56**:587-592.
17. Agrawal D, Cheng J, Seegopaul P, Gao L: **Grain growth control in microwave sintering of ultrafine WC-Co composite powder compacts**. *Powder Metallurgy* 2000, **43**:15-16.


## Acknowledgements

The author(YD) thanks Dr. Bjorn Sjodin of COMSOL Inc. for helpful discussions.